

An examination of estuary stability in response to human interventions in the South Branch of the Yangtze (Changjiang) estuary, China

Min Zhang^{a,c}, Ian Townend^b, Yunxuan Zhou^c, Lihua Wang^d, Zhijun Dai^{c,*}

^a School of Environmental and Geographical Sciences, Shanghai Normal University, Shanghai, 200234, China

^b School of Ocean and Earth Sciences, University of Southampton, University Road, Southampton, SO17 1BJ, UK

^c State Key Laboratory of Estuary and Coastal Research, East China Normal University, Shanghai, 200062, China

^d College of Resources and Environment, Chengdu University of Information Technology, Chengdu, 610225, China

ARTICLE INFO

Keywords:

Yangtze (Changjiang) estuary
Reclamations
Stability
Energy

ABSTRACT

Estuary morphologies are dynamic systems, and their stabilities are dependent on various forcing conditions, including tides, waves, and fluvial inputs. However, during the past half century, massive anthropogenic interventions have occurred in many estuaries around the world, resulting in substantial changes in morphologies. Here, we examine such changes in the Yangtze estuary to study decadal morphological stability under anthropogenic disturbances using an entropy-based approach. Using a numerical model, the influence of bathymetric changes and sea-level rise on the variations in energy within the South Branch was examined. An analysis of the spatiotemporal bathymetric variations suggested that the South Branch can be subdivided into three segments of the lower, middle and upper reaches. The changes in these three segments relative to a theoretical equilibrium state were used to investigate and attribute the causes of change. It was found that (1) reclamation works in the South Branch during the last half century, primarily the Xuliujing reclamations (before 1980s) in the upper reach and the Changxing Island expansion (Qingcaosha Reservoir project, 2002–2007) in the lower reach, moved the system away from equilibrium by 2.5–3% in total, although the natural evolution between 1987 and 1997 restored some of the lost efficiency; (2) before large-scale reclamations, river flooding disturbed the system away from equilibrium by 3–6% in 1958, but this was mitigated by 1–2% due to the reclamation works that constrained the channel and deepened the subtidal area; (3) an entropy-based analysis suggested that the Xuliujing reclamation introduced a river constraint that influenced the reach ~20 km downstream, and by enclosing the Qingcaosha Reservoir, a tidal constraint was introduced that influenced the reach ~30 km upstream; and (4) morphological adjustment within the South Branch (a form of self-organization) has enabled the system to adjust to the imposed changes toward a new dynamic equilibrium, consistent with the prevailing constraints and forcing conditions. The results of this study demonstrate a method to determine estuary stability in the context of human interventions, and this method may be relevant to other estuaries subject to large-scale changes.

1. Introduction

Morphological stability can have important implications for estuarine environments, especially in deltas that are of enormous societal and ecological relevance (Syvitski et al., 2009; Nordhaus et al., 2018). According to the evolutionary classification of Dalrymple and Choi (2007), river flows, tidal motions and wave actions are generally considered to be the main natural forcing conditions that control morphological change and the stability of estuaries. However, during the last century, many anthropogenic activities have occurred in estuaries, such as reclamations, embankment construction, and waterway

excavation, at a sufficiently large scale to make human interventions an additional forcing factor (Syvitski et al., 2009; Nordhaus et al., 2018). This new emerging force can perturb the system and alter estuarine resilience to other forcing conditions, such as sea-level rise (SLR) and thus raises important questions concerning their fate in a changing climate.

Numerous models of varying complexity have been used to study the stability of estuaries. These models are as follows:

- behavior-oriented models (Dronkers, 1986; Nicholls et al., 2016), which seek to explain estuary adjustment to changes based on

* Corresponding author.

E-mail address: zjdai@sklec.ecnu.edu.cn (Z. Dai).

<https://doi.org/10.1016/j.ecss.2019.106383>

Received 26 January 2019; Received in revised form 15 August 2019; Accepted 16 September 2019

Available online 16 September 2019

0272-7714/ © 2019 Elsevier Ltd. All rights reserved.

- process-based models (van der Wegen and Roelvink, 2008; Zhou et al., 2014; Luan et al., 2017), which represent the tide, wave, current and sediment transport processes to compute morphodynamic changes over time.

Such models are now well developed and have been shown to be capable of predicting long-term changes (van der Wegen et al., 2008) or the response to well-defined perturbations (Wang and Townend, 2012). The introduction of large perturbations has also been the focus of extensive modeling efforts in support of development proposals. However, post-development responses derived from modeling results do not always capture the morphological change that actually occurs for several reasons, such as environmental constraints or human disturbances (McLaren, 2013, 2016). Consequently, there is still much to be learned from the primary “data-driven” models, i.e., analyzing historical bathymetries and the corresponding hydrologic state to identify the influence of human interventions (Dai et al., 2013; Wang et al., 2013). An alternative approach proposed by Leopold and Langbein (1962) determines geomorphological stability based on entropy production and “optimality”, which is essentially a behavior-oriented approach. This approach was first applied to the landscape evolution of rivers (Yang, 1971) and then to other areas, including drainage basins (Rodríguez-Iturbe and Rinaldo, 1997), beaches (Bodge, 1992), tidal inlets (Niell et al., 2005), estuaries (Townend and Dun, 2000) and most recently to river deltas (Tejedor et al., 2017), all for natural forcing conditions. This approach has already been used in both the Yangtze River (Huang et al., 2014) and the Yangtze estuary (Zhang et al., 2016a), but little work has been conducted on a portion of the South Branch that is strongly influenced by river and tidal action, which has recently been subjected to intensive human interference.

The South Branch, which is the first-order bifurcation of the Yangtze estuary, was in a natural state over a long period of time until land reclamation projects were implemented beginning in the 1960s (Wang et al., 2013). Estuarine studies typically focus on the reach downstream of Datong station (Fig. 1a), which is approximately 600 km from the mouth, where there is a gauging station that denotes the approximate location of the upstream tidal propagation limit. Downstream of Xuliujing (Fig. 1c), the estuary branches into the North Branch and the South Branch. Further downstream, the South Branch divides into the North Channel and the South Channel. Finally, the North Passage and the South Passage form the main channel through the large subaqueous delta at the mouth of the estuary, which has a width of ~90 km (Fig. 1b). This well-defined branching channel structure has been shown to be a consequence of the prograding delta (Gao, 2013). Prior research on the South Branch has identified its important role in the sediment transport pathway (Yang et al., 2007), tidal propagation and river discharge passage (Guo et al., 2014; Luan et al., 2017) between the upper and lower reaches. Therefore, the sustainable development of the geomorphology of the South Branch is crucial in determining the evolution of the entire delta.

However, during the last century, numerous anthropogenic works have been conducted around the Yangtze estuary. These include large projects, such as land reclamations in Xuliujing and around Changxing Island, a water resource project for the Qingcaosha Reservoir, a deep-water channel deepening project, and embankment, dam construction and waterway dredging in the upstream regions (Yang et al., 2007; Xu and Milliman, 2009) and near the mouth (Dai et al., 2013). Some of these projects have directly influenced the South Branch (Wang et al., 2013), while others located outside the South Branch may have indirect effects. Therefore, scholars have argued that anthropogenic activities (disturbances) may have had more significant effects on the geomorphological evolution of the estuary than those due to natural forcing factors (Wang et al., 2013; Nordhaus et al., 2018; Zhang et al., 2018b) because the ability to adjust naturally to changes has been constrained by various engineering projects. As a result, there remains a need to

understand the effect of some of the important engineering projects on the recent morphological evolution of the Yangtze estuary.

In this paper, the primary focus is on the portion of the Yangtze estuary (the South Branch) just north of Shanghai, which is primarily influenced by the river and tide because this is the most socially and economically important reach and represents the main feature of the morphological evolution of the Yangtze River outlet. The morphological and hydrological changes over the last 50 years are considered based on a series of historical maritime charts and application of a hydrodynamic model. The results are used to examine the system behavior and in particular, the energy to assess the degree to which the system has responded to the imposed changes (Xuliujing and Qingcaosha Reservoir construction). By determining whether the system is locally and globally moving toward or away from the most probable state, the observed changes on a decadal time scale are related to the system behavior. A key component in this interpretation is the role of human disturbances and the ability of the system to recover from large-scale perturbations.

2. Methods

2.1. Data acquisition

The bathymetry data were sourced from historic measurement records, navigation charts, in situ observed data, the GEBCO (General Bathymetric Chart of the Oceans) database, archived remote sensing images, and previous literature results. These data were incorporated into a homogenous database by triangulated assimilation using a geographic information system (Zhang et al., 2016b, 2018a). In all, four historical navigation charts for 1958, 1987, 1997 and 2007 covering the South Branch and extending out to the bar area (Fig. 1b) and a navigation chart for 2008 covering the lower reaches of the Yangtze River (Fig. 1a) were collated. These charts were provided by the Maritime Survey Bureau of Shanghai (MSBS). Dual-frequency echo sounders were used for depth information (vertical error of 0.1 m). All depth points were digitized and expressed relative to the Huanghai1985 datum. Then, these points were projected from WGS1984 geographic coordinates to UTM Zone 51 coordinates. Shoreline positions were set at dikes or land-sea boundaries obtained from archived Landsat MSS/TM data taken at spring tide (<http://glovis.usgs.gov/>, accessed on 11th August, 2019). These were assigned the elevation of high water (Wu et al., 2002) to help define the intertidal zone.

After correcting the bathymetries to a consistent datum, the depths were modified to account for SLR. These adjustments were determined as relative changes from the earliest dataset (1958). An estimate of the annual SLR was based on previous literature results, which collectively suggested a rate that is approximately 1.9 times faster than the global average rate due to several regional factors (Shi et al., 2000). Early estimates of SLR for the region ranged from 2.1 to 2.5 mm/y (Liu, 1992), whereas more recent estimates (post 1990) using satellite altimeter data suggest a higher rate of 5–6 mm/y (Gong et al., 2012). Relative to the 1958 sea level, depth increases of 0.084, 0.127, and 0.176 m were applied to the 1987, 1997 and 2007 bathymetries, respectively (Shi et al., 2000).

2.2. Model setup

To examine tidal propagation under changing conditions (spring-neap, wet-dry season), a 2D numerical model was constructed using TELEMAC software. The model was configured with horizontal spatially varying triangular meshes, resulting in approximately 30,000 meshes and 23% of the elements located within the study area (Fig. 1a and b). To closely fit the changing historic shorelines, the grid layout in the area not affected by reclamations was kept constant; only the grid cells falling within the reclaimed areas were changed (added or removed) in the sequence of historic bathymetries. The available

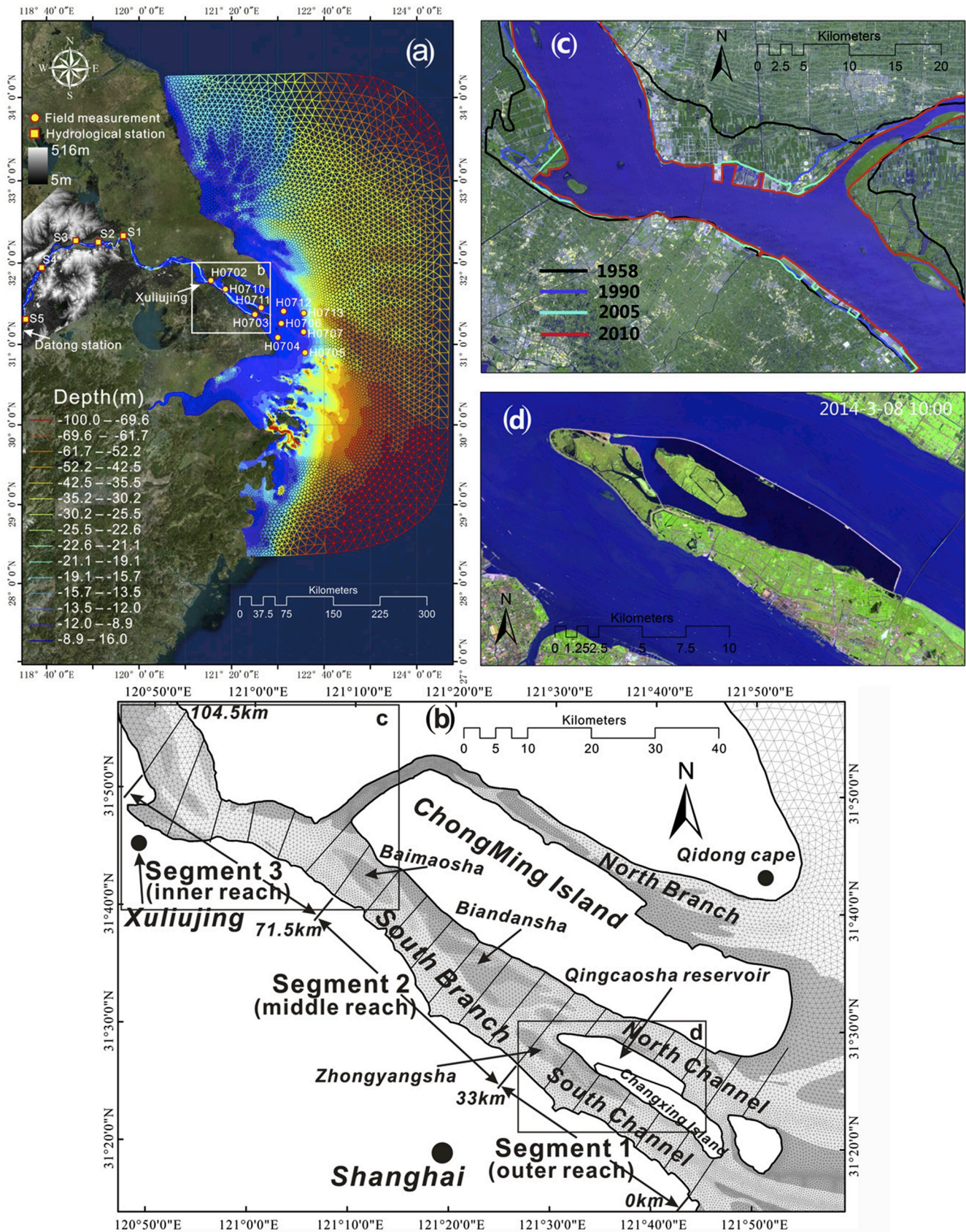


Fig. 1. (a) Sketch map of the triangular mesh for the entire modeling area in 2007, enlarged view at (b) the South Branch showing the 2007 shoreline, position of 5.5 km cross-sections and the 3 segment reaches, (c) remote sensing image at Xuliujing and historic changes in shorelines, and (d) recent remote sensing image of the Qingcaosha Reservoir.

bathymetries for historic analysis only covered the outer 100 km of the estuary and part of the mouth-bar area. However, the interaction with the river flow is critical for understanding the overall behavior of the system. Therefore, a detailed bathymetry using charts from 2005, 2007 and 2008 was created for the entire model domain (Fig. 1a).

The river boundary was set at Datong station. Daily river discharge data collected at this station during the 1950–2010 period by the Yangtze River Estuary Survey Bureau of Hydrology and Water Resource were used to define the representative river flow conditions. For the wet season, a discharge of 35,000 m³/s was used, whereas 15,000 m³/s was used for the dry season. These define the typical conditions. In very dry periods, there is almost no run-off and the river boundary was set to a flow rate of 1,000 m³/s for this condition. At the other extreme, peak flows can be much larger, and a value of 60,000 m³/s was used in the model to represent spate conditions. The flow conditions do not appear to have changed significantly despite the addition of many dams further upstream (Xu and Milliman, 2009). Thus, these conditions were used for all four epochs.

The seaward boundary, which is defined using the tides obtained from TPXO (TOPEX/POSEIDON global tidal model dataset), was set at a substantial distance offshore (~150 km) to avoid boundary effects in the model (Fig. 1a). The ocean tide in the Yangtze estuary has a well-defined spring–neap cycle (Haigh et al., 2011), and a representative annual spring–neap tidal cycle was extracted from the TPXO7.2 dataset, using the method of Latteux (1995) to define the representative harmonic constants. This allowed all the simulations to be conducted using the same tide to force the seaward boundary. In the runs of each bathymetry epoch reported here, all model parameters and boundary conditions were held constant; only the bathymetry was changed (although this includes a variation due to SLR, as was already explained).

2.3. Model calibration and validation

Data for water levels and flow speeds collected offshore and upstream of Xuliujing during July 2007 as well as 5 gauging stations in the river reaches (as far as Datong station) were used to first calibrate and then validate the model (Fig. 1a). The results of the model calibrations and validations for dry and wet seasons are presented in Zhang et al. (2016a), and the results for neap and spring tides are presented in Zhang et al. (2016b). Statistical errors (e.g., RMSE) of the modeling results are presented in Table 1. Careful calibration enabled the model parameters to be defined for all simulations, including the hydrodynamic time step (90 s), the Nikuradse bottom frictional coefficient (0.001 m), and the horizontal diffusion velocity coefficient (0.1). These parameters were used for all subsequent runs, with the outer 100 km mouth–reach replaced with the bathymetry from each epoch. Details of the model configuration and calibration have been reported elsewhere (Zhang et al., 2016a, 2016b; 2018a,b), together with an analysis of how the system adjusts in response to the seasonal variation in river discharge.

2.4. Analytical metrics

2.4.1. Morphological parameters

Each bathymetric dataset was used to examine the four river flow

conditions with a representative spring tide. The model output, which comprised water levels and flow velocities, was then processed to derive several metrics. For this analysis, a series of cross-sections were defined at approximately 5,500 m intervals along the South Branch (Fig. 1b). At each cross-section, water levels and velocities normal to the line were calculated as section averages, and the variation in the cross-section area with water level stage was computed. For each reach between two adjacent cross-sections, volumes and surface areas were obtained. These values were calculated using (i) a series of horizontal planes at specified intervals through the vertical to define a hypsometry, and (ii) relative to the high and low water surfaces to track changes in the channel and intertidal volumes. Notably, the high and low water surfaces were constructed from water levels at different times during the tidal cycle because the times of high and low water varied along the estuary.

2.4.2. Energy and entropy production

In this research, the energy flux was used to relate bathymetric changes and hydraulic conditions as captured by variations in surface elevation and flow velocities to evaluate estuary stability (Langbein, 1963; Townend and Dun, 2000):

$$F_B = uBE \quad (1)$$

where F_B is the energy flux (W or J/s), u is the flow velocity (m/s), B is the cross-section width (m), and E is the energy head per unit width (J/m²), which is a function of the water surface elevation, channel depth, and flow velocities due to river, tide and river–tide interactions (Zhang et al., 2016a). The energy flux given by equation (1) is a time-dependent value; when integrated over a tidal cycle, the result is the total energy passing through the cross-section (units of Joules).

For landscape evolution in a hydrographic system near equilibrium, it has been suggested that the entropy production per unit volume will tend to evolve to a minimum that is compatible with the constraints (such as human intervention or hard rock geology) imposed on the system (Leopold and Langbein, 1962; Langbein, 1963). Applying the concept of minimum entropy production per unit discharge to the more general case of a bidirectional variable discharge along a channel reach suggests that the theoretically “most probable” energy distribution along an estuary can be determined as follows (Townend and Dun, 2000):

$$\int F_B dt = D \cdot \exp(C \cdot x) \quad (2)$$

where x is the distance from the mouth, and C and D are constants. For this study, the constants C and D were obtained using a least-squares regression over the entire length of the South Branch (104 km). By integrating over a tidal cycle, the boundary condition is cyclic and therefore meets the requirement of being approximately stationary. If the total energy flux under real conditions computed via equation (1) is greater than the theoretically most probable state determined by equation (2), then the system is too large and should evolve to be smaller, while the opposite indicates that the system is evolving to become larger. Therefore, our analysis examined the changes in (i) energy flux (J/s), (ii) total energy (J) and (iii) so called ‘distance from most-probable’ (%) over time. The latter is simply the difference between the actual and theoretical energy fluxes over a tidal cycle,

Table 1

RMSE of modeled and measured data at both the estuary (H) for spring and neap tides and the upstream hydrological stations (S) for dry and wet seasons. Refer to Zhang et al. (2016a), 2016b and 2018a,b for other stations.

Spring/Neap	H0702	H0703	H0704	H0706	H0710	H0711	H0712
Velocity	0.18/0.10	0.34/0.15	0.38/0.17	0.31/0.16	0.18/0.14	0.25/1.25	0.39/0.15
Elevation	0.38/0.20	0.49/0.43	n.a./0.12	0.15/0.08	0.35/0.15	0.44/0.49	0.42/0.22
Wet/Dry	S1	S2	S3	S5			
Elevation	0.10/0.12	0.11/0.08	0.12/0.10	0.09/0.08			

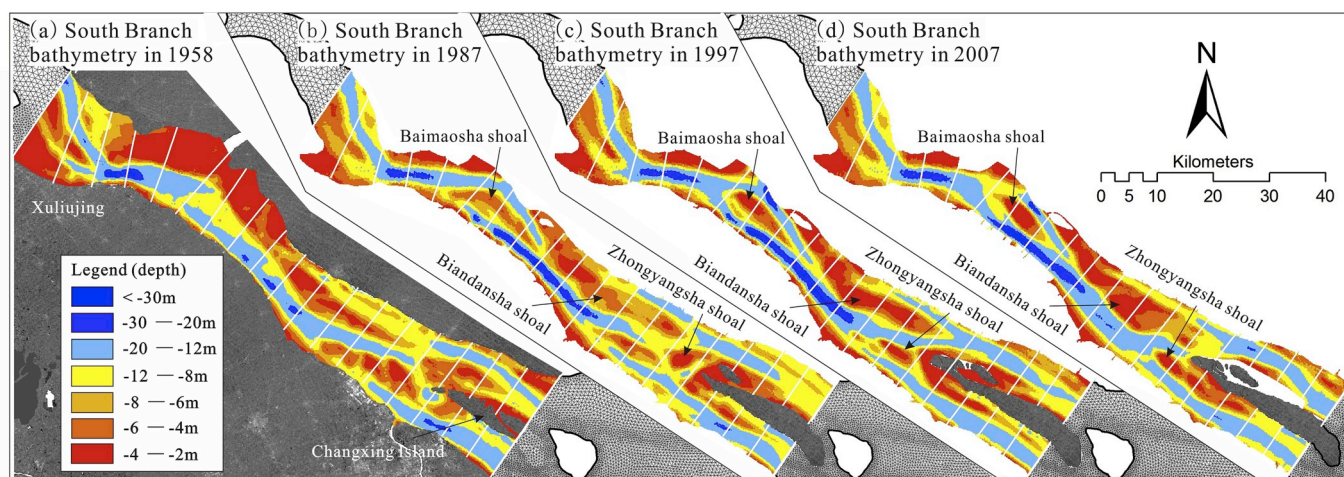


Fig. 2. Variation in bathymetry of the Yangtze estuary from the mouth to Xuliujing between 1958 and 2007.

integrated over the mouth reach.

3. Results

3.1. Morphology

3.1.1. South Branch bathymetric change

From the bathymetries compiled in Fig. 2, some notable changes are discernible, particularly the narrowing of the Xuliujing channel, the expansion of Changxing Island and the changes in the Biandansha, Baimaoshan and Zhongyangsha shoals in between these features. Then, for some of the analysis that follows, the area was subdivided into three segments: 0–33 km for Segment 1, 33–71.5 km for Segment 2 and 71.5–104.5 km for Segment 3 (see Fig. 1b).

Prior to the 1960s the width at Xuliujing exceeded 14 km (Fig. 2a). However, by the late 1980s, reclamation projects had reduced the width to only 6.9 km (Fig. 2b). Consequently, this short reach of the estuary (Segment 3) is now a much larger constraint on behavior. Prior to the reclamation projects, the width was sufficient for the channel to be able to move laterally and for shoals to move upstream and downstream (Wang et al., 2013). Since 1987, the narrow channel at this location has provided a disconnect between the upstream and downstream reaches, and this short reach has shown little volumetric change. Immediately downstream, the estuary widens again to over 11 km, and the Baimaoshan shoal has grown back since 1987 (Wang et al. (2013) showed that this shoal was extensive and varied in size prior to the 1950s).

Similarly, the outer reach (Segment 1), which constitutes the Changxing-Zhongyangsha system, has also been reduced in width. With the Changxing Island expansion from 1958 to 1997, intertidals have been reclaimed, and shallow shoals have been growing laterally, taking over the deep channel areas on both sides. Moreover, channels deeper than 12 m have extended by 35% in the plan area. With the Qingcaosha construction in 2007, the intertidal region to the north of the island was almost entirely lost, while channels deeper than 12 m have been continuously becoming wider and straighter. Immediately upstream is Zhongyangsha, which has continuously evolved from 1958 to 1997 to be smaller and attached to the area south of Changxing Island in 2007.

In contrast, the reach in between (Segment 2), which constitutes the large Baimaoshan-Biandansha system, is still free to adjust. The channel to the north of Baimaoshan increased in depth from 12 m to approximately 20 m and extended downstream from 1958 to 1997. More recently, the channel has infilled, reducing depths to the north of the shoal to approximately 10 m. The channels to the south of Baimaoshan and Biandansha have also become straighter and deeper, and by 2007,

these channels extended southeastward to the upper end of Changxing Island. Biandansha has become much shallower and more extensive while also migrating downstream. By 2007, Biandansha extended to Changxing Island with a shallower connection between the Biandansha channel and the North Channel, whereas the shoal between the Biandansha channel and the South Channel had disappeared.

The volume relative to high water over the entire South Branch, representing the total bathymetric volume, and the volume change due to SLR are shown in Table 2. The SLR volumes are small when compared with the total bathymetric volume (less than 1%). However, their rates of change are of a similar order of magnitude but with opposite signs (at least until 1997). This finding implies that the morphological change is substantially greater and is offsetting the increase in volume due to SLR. Although it is conceivable that the system will infill at a rate commensurate with SLR (Townend et al., 2007), such that the total volume remains approximately constant, the changes in the South Branch of the Yangtze estuary suggest a much faster rate of infilling—approximately 6–10 times faster than the rate required by the SLR volume changes.

3.1.2. Hypsometric changes

For each of the segments identified in Fig. 1, the plan area at specified intervals through the vertical were derived from a digital elevation model (DEM) for each year to determine the sectional hypsometric changes over time (Fig. 3). Starting from the upstream end, the changes in Segment 3 were significant. The maximum depth was unchanged. However, the segment has narrowed significantly above –12 mAD and widened below it, indicating a smaller intertidal region and a wider deep channel. Similarly, Segment 2 showed nearly the same trend.

Table 2

Total volume below high water and volume change due to sea level rise (SLR).

Year	1958	1987	1997	2007
Volumes and rates				
Total volume (m^3)	1.64×10^{10}	1.52×10^{10}	1.49×10^{10}	1.46×10^{10}
Total rate of change (m^3/yr)		-4.04×10^7	-2.57×10^7	-3.18×10^7
SLR volume (m^3)	0	1.18×10^8	1.73×10^8	2.24×10^8
SLR rate of change (m^3/yr)		$+4.08 \times 10^6$	$+5.44 \times 10^6$	$+5.17 \times 10^6$
Morphological rate of change (m^3/yr)		-4.45×10^7	-3.12×10^7	-3.69×10^7

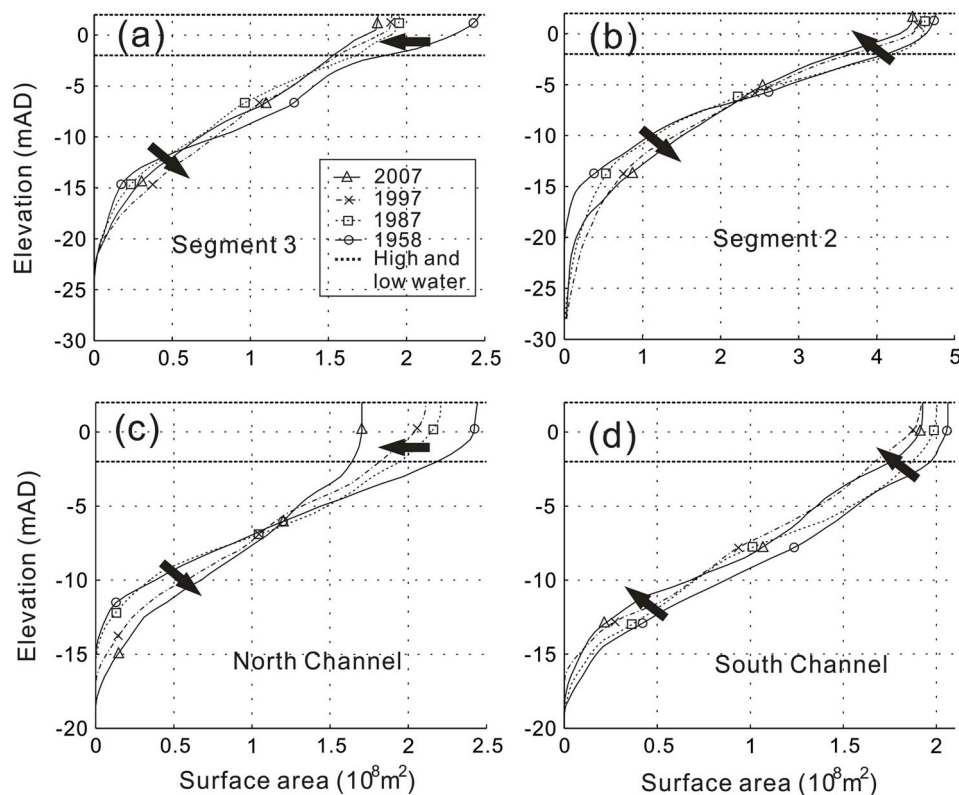


Fig. 3. Variation in hypsometry over time based on the 3 Segments, with the outer segment subdivided into the North and South Channels. The dotted horizontal lines represent high and low water levels, and the elevation is measured relative to the Huanghai1985 datum (mAD is meters above datum).

Overall, the segment became significantly deeper in terms of its maximum depth and the extent of the channel below -7 mAD. In contrast, the area above this level exhibited shoaling by a similar amount at all levels up to the high water level, indicating a narrower and deeper channel morphology. These changes are consistent with those reported by Zhao et al. (2018).

The pattern of change in the North Channel is similar and shows a clear progression over time. There has been an anticlockwise rotation of the hypsometric profile such that the channel is larger and deeper below -7 mAD and smaller and shallower above this level. Overall, there has been a progressive narrowing and deepening of this channel. Changes between high and low water are also more significant in the North Channel, resulting in a notable loss of intertidal area. In contrast, the South Channel has seen a reduction in plan area over all depths so that the hypsometric profile for the South Channel has an approximately constant shape but with a plan area that is reducing in magnitude over the entire water column over time. Hence, the channel is narrowing and becoming shallower.

3.2. Reclamations and area/volume change

The effect of human activities on estuary morphological development has been significant in the South Branch of the Yangtze estuary. Land reclamation and construction of artificial islands in this area occurred throughout the 50-year study period, as shown by the coastline and reclamation area changes shown in Fig. 4a and b. In total, over 440 km^2 have been reclaimed within the South Branch, accounting for over 27% of the pre-reclamation plan area. The areas and volumes reclaimed in each segment during each period are depicted in Fig. 4c and d. The largest reclamation occurred during the 1958–1987 period, when 240 km^2 of surface area was reclaimed, with the 1960s Xuliujing reclamation accounting for $\sim 70\%$ of the total that took place during this period. The second largest reclamation works were conducted from 1997 to 2007, when 140 km^2 was reclaimed, predominantly during the

2000s Qingcaosha Reservoir construction, which accounted for $\sim 60\%$ of the total. The changes in the area and volume of the estuary at or below $+2$ mOD for each segment are shown in Fig. 4e and f. These plots also show the amount of reclamation as a proportion of the initial value in each interval.

Overall, reclamation reduced the intertidal volume significantly throughout the estuary, with more taken at both ends of the South Branch than the middle segment (Fig. 4c and d). As a result, the total channel volume was reduced, although the volume at low water levels increased slightly in Segments 2 and 3, indicating a deeper and narrower morphology in this reach. The plan area changes are most significant between 1958 and 1987, amounting to a 14% change from the 1958 plan area (Fig. 4e). Changes between 1987 and 1997 were comparatively small ($\sim 3\%$) before an additional 5% was removed between 1997 and 2007. Volume changes are much smaller, as a proportion of the 1958 high water volume, with changes of $\sim 7\%$, 1.5% and 2.5% for each interval (Fig. 4f). This is not surprising given that most of the removed areas are intertidal and therefore relatively shallow. However, the loss of volume is likely to be more significant under higher flow conditions, especially floods, when the intertidal area provides valuable additional storage volume in proportion to its plan area.

3.3. Energy flux variation

3.3.1. Two-dimensional energy flux change

The tidally averaged energy flux per unit width (based on $F = uE$ in each grid cell integrated over a tidal cycle) is shown for the four river flow conditions and four time periods in Fig. 5. The most marked difference is between the peak flow conditions and the other conditions, particularly at the upstream end of the reach. Under peak flows, the region of intense energy flux expands to occupy most of the width and extends alongside Biandansha shoal, almost as far as Changxing Island. The other three cases all have less extensive, more fragmented areas of maximum flux, leading to a more even distribution of energy flux in the

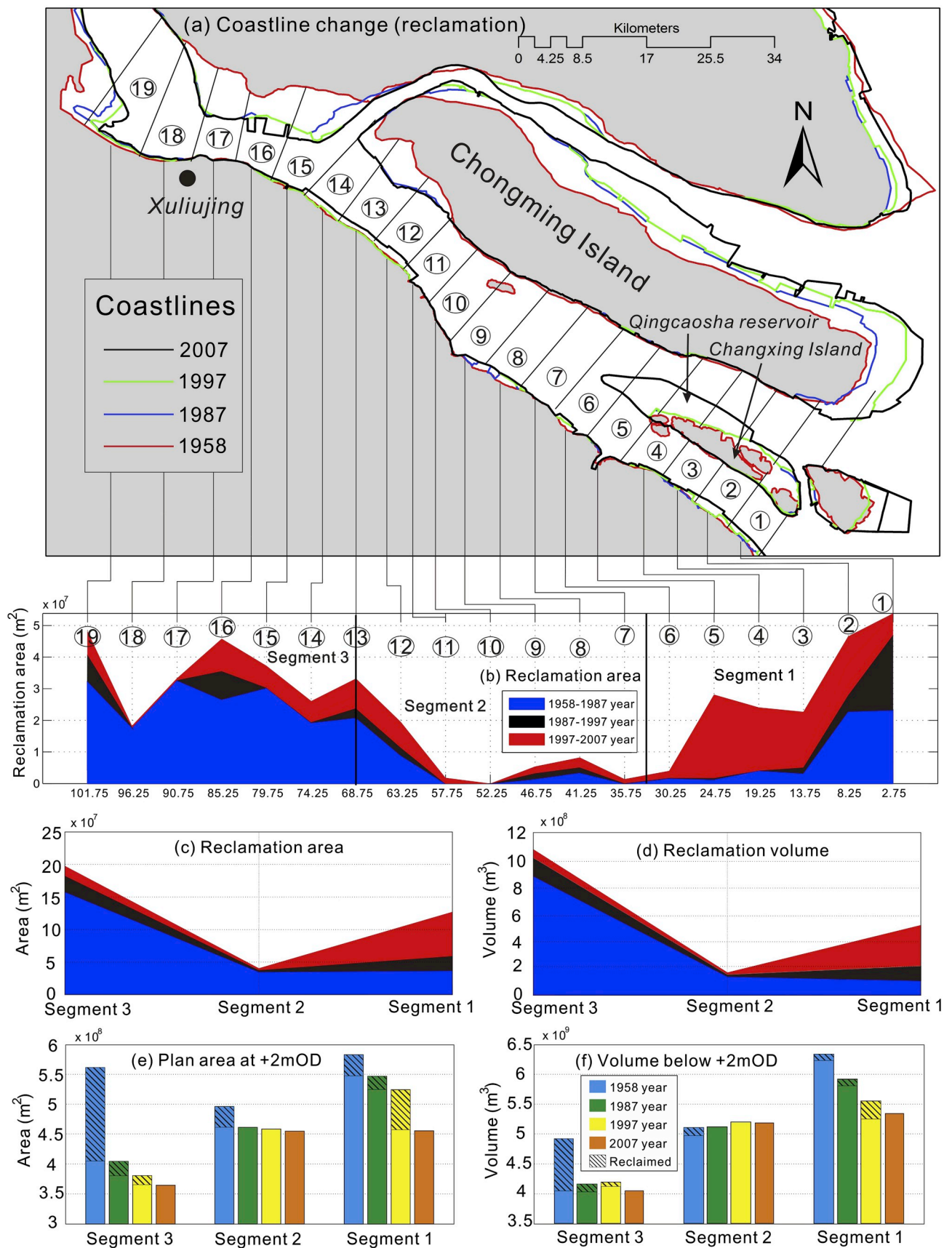


Fig. 4. (a) and (b) historical coastline changes and along-channel reclamation area variation derived from archived remote sensing images and navigation charts, (c) and (d) reclamation area and reclamation volume change over time for the three segments, and (e) and (f) the water area and volume relative to +2mOD. The shaded area of the bars is the area or volume removed due to reclamation that had occurred by the time of the subsequent survey.

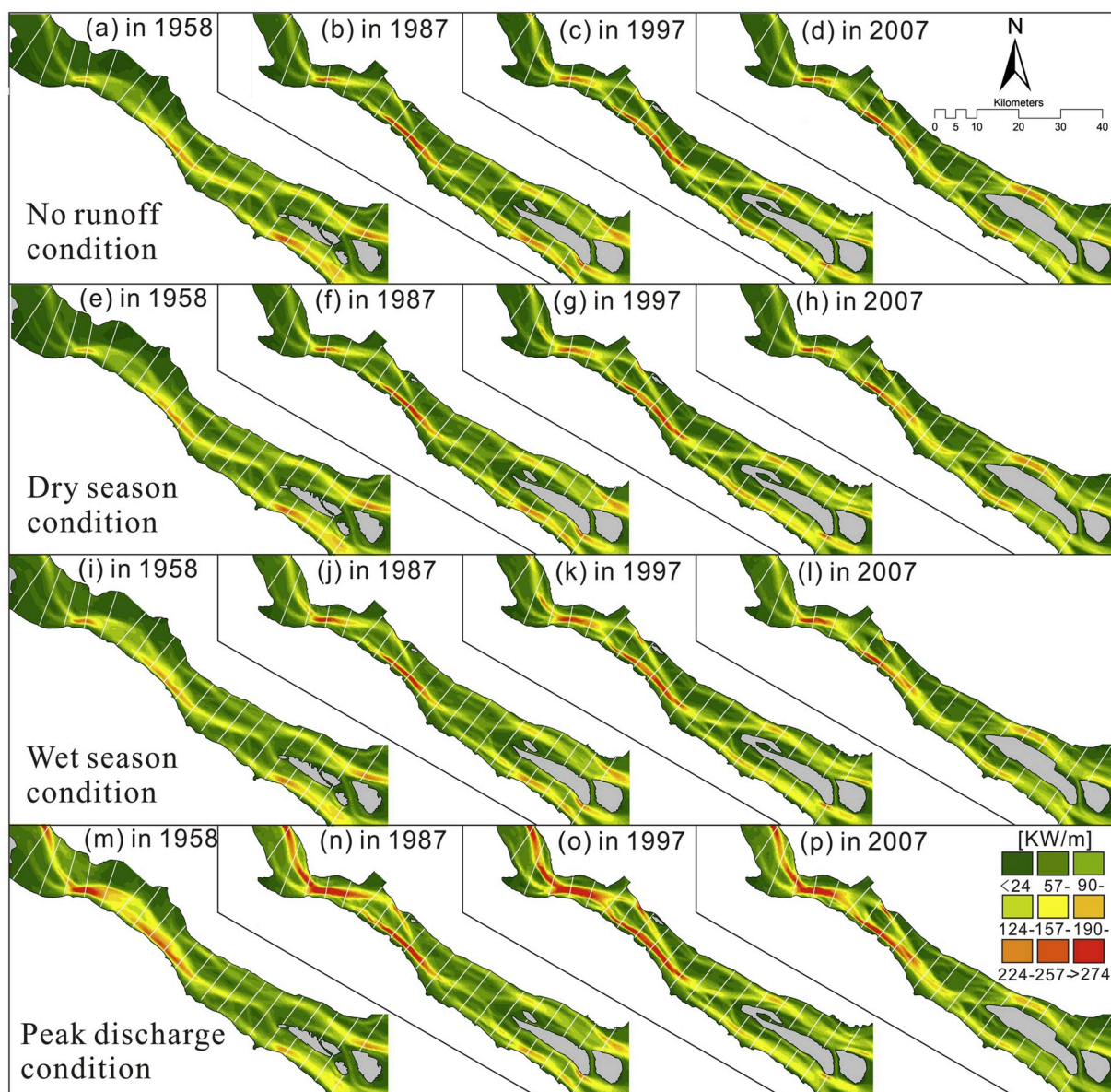


Fig. 5. Variation in tidally averaged energy flux per unit width in the South Branch of the Yangtze estuary under a range of flow conditions, showing variations over the studied period (1958–2007).

South Branch.

More specifically, in the outer reach near the mouth (Segment 1), some notable changes occurred over time. As Changxing Island has been progressively reclaimed, the intensity of the energy flux in the South Channel has decreased, which has been compensated by an increase in the flux through the North Channel. This change is superimposed on the variations in river flow conditions. Under tidally dominated conditions, the intensity of the flux in the North and South Channels is comparable. However, as the river discharge increases, there is a greater asymmetry between the two channels. During the early period, there was a higher energy flux through the South Channel; however, more recently, this flux has shifted to favor the North Channel. Moreover, in the middle reach (Segment 2), the main flux is on the south side, which intensified between 1958 and 1997. Then, the main flux became more diffuse but more extensive by 2007, notably to the south of the Baimaoshao shoal. Further upstream, in Segment 3, the flow is in a wider channel, the energy flux is diffuse and there was almost no gradient around Baimaoshao in 1958. By 1997, gradients that demarcate the main channels were established. This change was likely

the consequence of the combined influence of the major flood in 1954 (Wang et al., 2013) and the reclamation projects near Xuliujing before the 1980s, which as seen in Fig. 2, flushed the shoal away. The shoal had begun to re-establish itself by 1987 and was fully formed again in 1997.

3.3.2. One-dimensional energy flux change

A description of energy propagation along the channel was obtained by integrating the energy flux over transverse cross-sections extracted at 200 m intervals along the channel. The variations under the four flow conditions, in each epoch, are presented in Fig. 6c–f. These fluxes are compared with the theoretically ‘most probable’ distribution of tidal energy represented by equation (2). The residual differences between the estimated (real) and theoretical (exponential) energy flux along the channel were used to obtain the average percentage difference from the most probable state. The values varied by approximately 3–5%, although differences as high as 11% were found under peak discharge conditions.

Overall, it is apparent that the actual distribution of the total energy

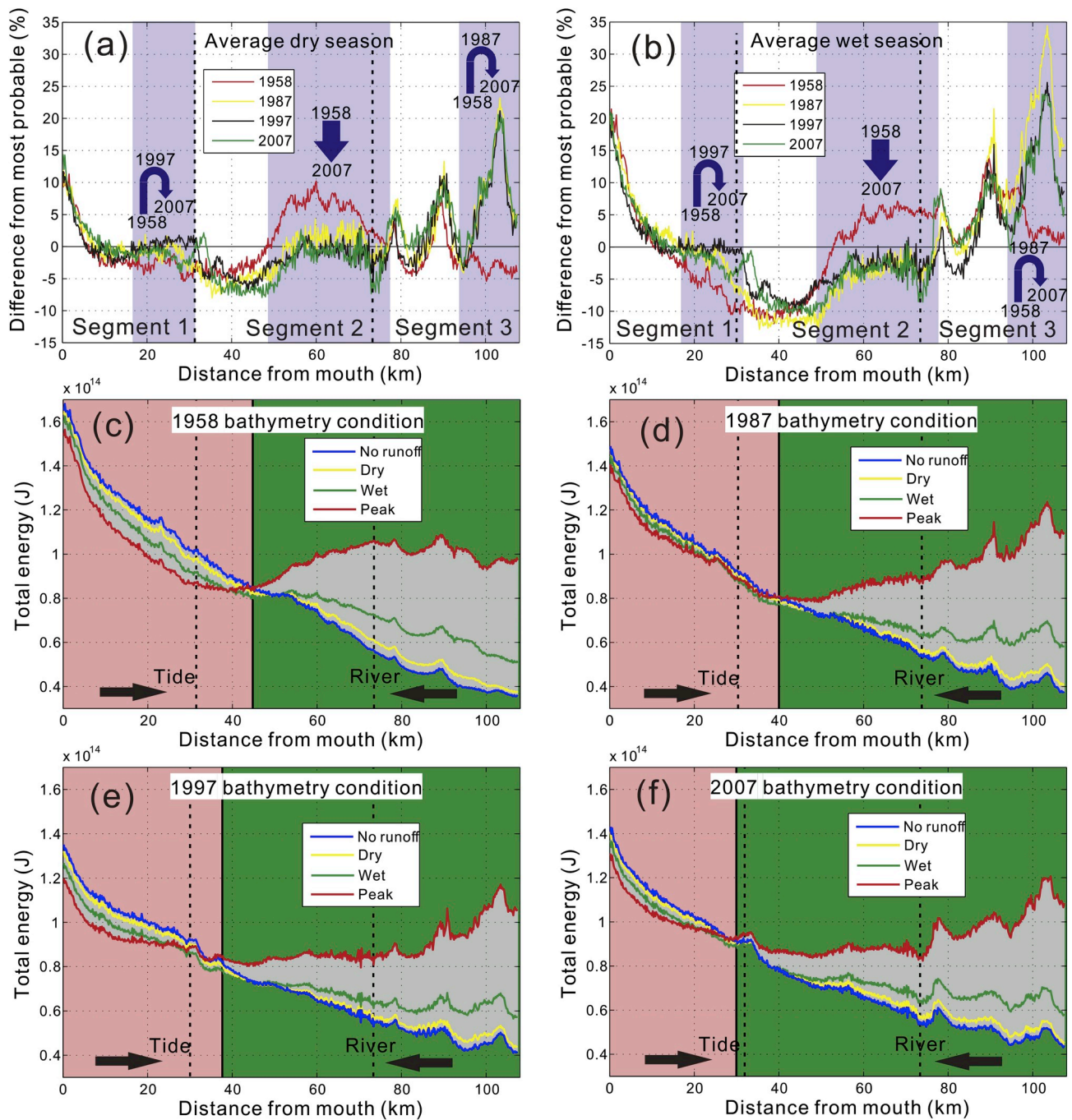


Fig. 6. Difference in the total energy from the most probable (exponential) energy along the estuary for different years under (a) typical dry season and (b) typical wet season conditions. Lengths over which there is a clear temporal progression are shaded, and the changes are identified by the solid arrows. The distribution of the total energy flux (tide and river) over a tidal cycle along the estuary for a range of river flow conditions are shown for (c) 1958, (d) 1987, (e) 1997 and (f) 2007. The black dotted lines indicate the division of the 3 segments. The black solid line is the transition between the river and tide, with the river-dominant reach to the right of the line and the tide-dominant reach to the left.

flux decays exponentially in the upstream direction along the South Branch (Fig. 6c–f), except under peak flow conditions, as the total energy flux exhibits a reversal 40 km from the mouth. For peak river discharges (red line), the total energy in the upper reach is dominated by the energy from the river, and, in the lower reach, it exhibits a minimum compared with the other river discharge conditions, mostly due to intensive river-tide interactions (Guo et al., 2014; Zhang et al., 2016a). The transition from river dominance to tidal dominance moved gradually downstream from 45 km in 1958 to 40 km in 1987 and further to 38 km in 1997 and 30 km in 2007, which was mostly due to

repressed tidal propagation by the river. Because all other boundary conditions were constant, it follows that the change in bathymetry, including changes in depth due to SLR, was responsible for the shift in the river-tide transition.

Another important change is the reduction in energy input from the ocean over the last 50 years, albeit with a small recovery in 2007 (values at the mouth in Fig. 6c–f). This change was also reflected in the coefficient, D , a measure of the energy at the mouth, which decreased from 1958 to 1997 but remained approximately constant from 1997 to 2007. Furthermore, a reduction in total energy over the tidal reach, as a

function of increasing flow conditions, is notable in 1958 and 1997 but less distinct in the other years.

3.4. Energy dissipation

When examining river networks and estuaries, the principles of uniform energy dissipation (a local condition) and minimum energy expenditure in the system (a global condition that results in minimum work) have been extensively explored (Leopold and Langbein, 1962; Rodríguez-Iturbe and Rinaldo, 1997; Townend and Dun, 2000). These two measures are used to examine the changes in the South Branch.

3.4.1. Uniform energy dissipation

An exponential variation in energy flux over a tidal cycle (total energy) implies uniform energy dissipation. The percentage differences from the theoretical exponential decay, shown in Fig. 6a and b, therefore provide an indication of the extent to which this condition is met. Where segments deviate from the most probable state indicates that the combination of bathymetry, hydraulics and system constraints are no longer consistent with the uniform energy dissipation argument. To summarize the local changes in energy dissipation over time, the focus is on the typical dry (winter) and typical wet (summer) season conditions (Fig. 6a and b). The no runoff and peak discharge conditions are included in this analysis to indicate the range of energy changes in the system, as shown by the gray background in Fig. 6c–f.

Generally, the results agree with the principle of uniform energy dissipation (Fig. 6a and b). Under both flow conditions and for all years there is a deviation at the mouth (0–10 km) that remains largely unchanged over time. This may be a consequence of only considering river and tidal energy in an area where wind-wave energy may also be significant. In addition, there are three consistent patterns present, as indicated by the arrows and year markers in Fig. 6a and b. In Segment 1, there was a move towards the ‘most probable’ between 1958 and 1997 and a move away in 2007. The opposite occurred in Segment 3, with a move away from the ‘most probable’ in the 1958–1987 interval and a subsequent return after 1987. A very different pattern is apparent in Segment 2, where 1958 is clearly a perturbed state. This deviation is presumably driven by events that occurred prior to the study period and may be a consequence of one or more large flood events. Subsequently, there has been a move back toward the ‘most probable’ state. Over the same period, the low water channel reduced by approximately 230 Mm³ in volume, while the total channel volume decreased by nearly 1,750 Mm³, mainly due to the loss of intertidal area (the plan area decreased by 363 km²).

3.4.2. Minimum work

Another way of investigating the Yangtze estuary stability that is consistent with the entropy-based argument is to examine the difference between the total energy (river and tide) entering and exiting the system to define the energy contribution to the work done globally (Nield et al., 2005). Again, it is useful to investigate how this has changed over time; for simplicity, it is presented in terms of the energy dissipation ratio, as given by the difference between the total energy input (Fig. 7a) and energy output (Fig. 7b) divided by the total energy input, as shown in Fig. 7c. The overall decline in the amount of energy entering the system over time is clearly shown in Fig. 7a. This decline is accompanied by a commensurate reduction in the energy exported over the period but with a temporary increase between 1987 and 1997 and subsequently falling again by 2007, as shown in Fig. 7b.

Taken together, the total energy dissipation ratio shows a loss of efficiency (more dissipation as a proportion of the energy input) of 7–9% between 1958 and 1987, which reduced by approximately 8% from 1987 to 1997 and then increased by approximately 5% over the most recent interval. Notably, these changes are observed in the energy dissipation within the South Branch, regardless of the river flow conditions, as shown in Fig. 7c. For the larger flow conditions, the entropy-

based analysis reveals a similar trend, as shown in Fig. 7d. However, there are two important indicators revealed by the differences from the ‘most probable’ state. First, between 1958 and 1987, low flow conditions were unaffected (or even moved closer to the ‘most probable’ condition), whereas the high flow conditions moved away. However, in the 1997 to 2007 interval, all flow conditions moved away from the ‘most probable’. This finding implies that changes in the first interval reflect a change that is influenced by the river flow, whereas in the last interval, the change is the same for all flow conditions and hence are quite possibly tidally influenced. The second indicator is provided by the magnitude of differences for the various flow conditions. In 1958, higher flows strongly perturb the system away from the ‘most probable’ state. This amplification is enhanced in 1987 but then strongly dampened, such that in 1997 and 2007, the perturbation due to high flows appears to be less than in the earlier epochs.

4. Discussion

4.1. Impacts from anthropogenic interventions

In addition to natural forcing factors related to rivers, tides and waves (Dalrymple and Choi, 2007), there is growing evidence that anthropogenic interventions in the last half century had a major influence on the evolution of the Yangtze estuary (Wang et al., 2013). The land reclamation along the South Branch over the last half century has removed over 22% of the water surface area. Although some tidal flats (notably around Chongming Island) have accreted, the net change is a loss of nearly half the intertidal area. In the South Branch, most of the change is due to two episodes of construction, namely, reclamation around Xuliujing and construction around Changxing Island.

The first sustained episode of reclamation was in the late 1950s and early 1960s in the area at the head of the South Branch, which is near Xuliujing. The construction of artificial islands and land reclamation in this area reduced the estuary width from 14.5 km in the 1950s to 6.9 km. The reduced channel width substantially increased the local channel convergence, which likely led to enhanced bed erosion during high river flows. The eroded sediment, which was accompanied by suspended sediment from upstream, would have been transported downstream and is consistent with the subsequent accretion on the Baimaoshan shoals and the middle reach (Wang et al., 2013). Thus, the observed changes in the volume of this central reach may be the direct result of reclamations on both banks of the Xuliujing channel. It is also highly likely that there has been a discernible morphological response upstream of Xuliujing, although the data coverage is insufficient to investigate this further.

The other major change in estuary area and volume was close to the mouth because the shoals around Changxing Island were progressively reclaimed from the 1960s onwards and the Qingcaosha Reservoir (2002–2007) was constructed. Previous research has indicated that the project induced significant changes in terms of salt water intrusion (Zhu et al., 2013), estuarine circulation (Ge et al., 2013) and sediment transport (Guo and Zhu, 2015; Zhu et al., 2016). Before the project, accretion on the shallow shoals and erosion in the deep channels was moderate. After the project, extensive areas of the shoals were enclosed by levees, causing a narrowing of the North Channel from 9.8 km to 5.1 km and a continuous deepening of the channel. Then, the main channel and the Biandansha shoal, located approximately 30 km upstream, underwent progressive incision, bed scouring and development. The constraint of the North Channel also favored the development of the South Channel, although it has been claimed to have had a minor impact (Dai et al., 2016). Over this period, the changes in energy flux also suggest that the system has been perturbed away from equilibrium.

The impacts from other projects, such as the deep-water channel deepening project, could also have influenced the geomorphology of the South Branch. However, previous work has shown that the influences of such projects have been predominantly local because the

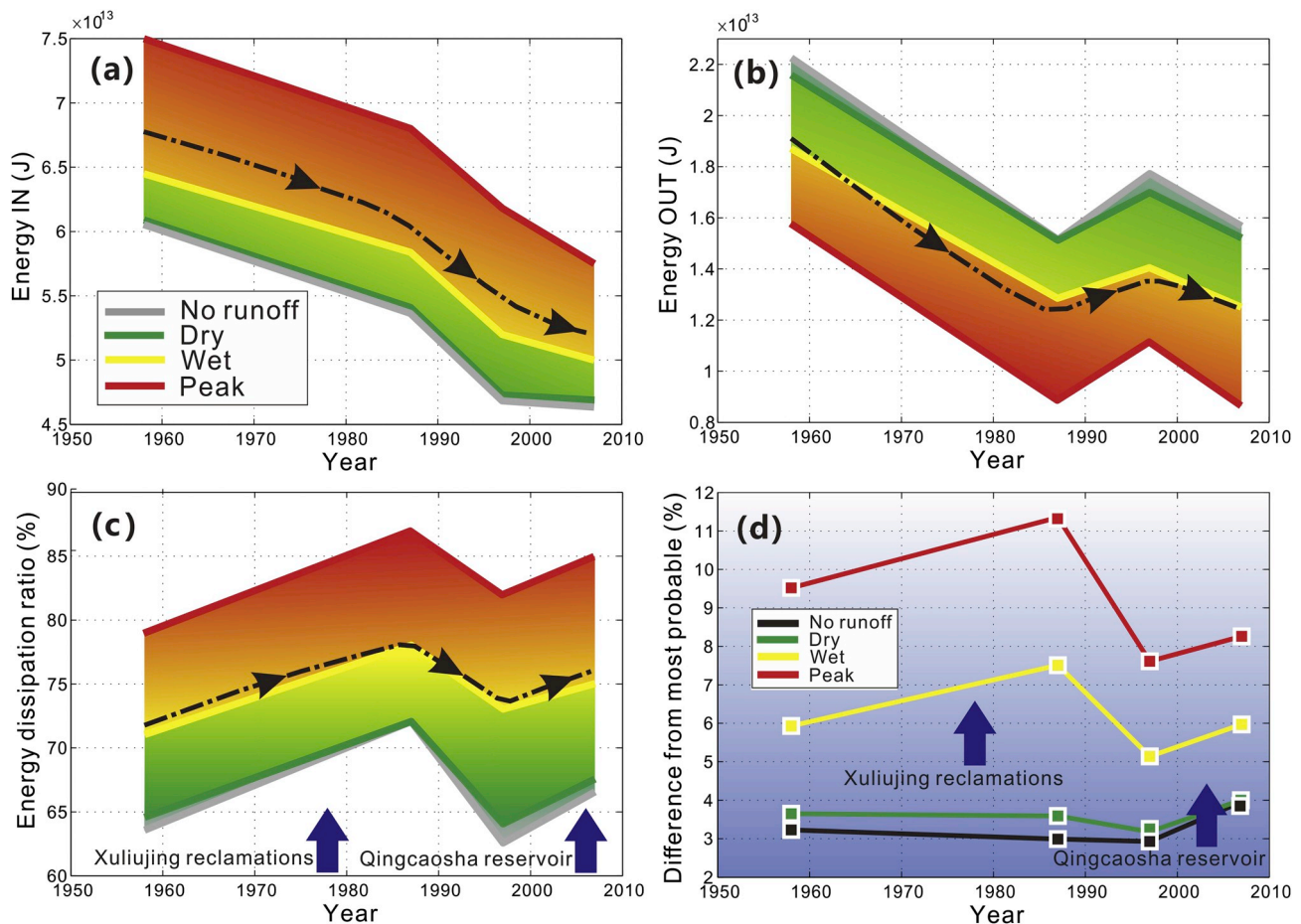


Fig. 7. Variation in the energy into and out of the South Branch of the estuary and the associated dissipation ratio and percentage difference from the most probable state over the studied period and for the different flow conditions examined.

construction projects have not significantly altered the sediment input and output (Wang et al., 2013). In contrast, large episodic floods can alter the channel conveyance and move large volumes of sediment (Cooper, 2002). Historically, this may have caused periodic shoreline movement before 1958 (Wang et al., 2013). However, seawalls now protect the shoreline around the reclaimed areas. Floods are only able to deepen the constrained channel, rather than spread it laterally. Any new tidal flat, formed during non-flood periods, was invariably subject to further reclamation (Dai et al., 2016). As a result, reclamation has changed the natural evolution, to progressively narrow and deepen the channel.

Upstream dams further complicate matters. While flows remain seasonally variable but of a similar magnitude, the sediment flux to the sea has been shown to have declined as a result of dam construction (Yang et al., 2007). Evidence to-date suggests that this has not reduced the potential for accretion in the tidal delta due to positive feedbacks between sediment deposition and tidal prism, as discussed by Zhang et al. (2018b), while other researchers have suggested that this is a cause of erosion in the inner estuary (e.g., Luan et al., 2016).

4.2. River and tide impacts superimposed on reclamations

The distance from the mouth of the South Branch to Xuliujing is over 100 km, and changes in the channel width at either end due to reclamation projects have been on the order of 10 km. Although extensive in plan area (160 km² and 85 km²), these changes have been spatially discrete and occurred at different times (separated by four decades). Since the reclamations are sufficiently large, they are expected to have distinct morphological influences. However, the effect of

reclamations on morphodynamics is combined with river flow and tidal signals. This has been the focus of much research, as modeled in this study, which is believed to govern the localized erosion and accretion in the South Branch (Wang et al., 2008; Guo et al., 2014). Wind waves are also present, but as waves decay rapidly inside the mouth due to the sheltering of Hengsha and Changxing Islands, they are not considered to have a significant influence (Zhang et al., 2018a).

The change in the energy flux in the South Branch in response to reclamations has also been quite distinct. The system performs most efficiently when the river influence is small (no runoff and dry river discharge cases in Fig. 7d). However, following the Xuliujing reclamations in the upstream segment, the change in efficiency was most apparent for high discharge events (wet and peak river discharge cases in Fig. 7d). Hence, it was asserted that this is river controlled. In contrast, following the Qingcaosha Reservoir construction close to the mouth, the system moved away from the prevailing state prior to 2007 for all four river flow conditions. This is consistent with the expansion around Changxing Island constraining tidal propagation and reducing system efficiency (Fig. 7). Therefore, the response to the upstream reclamation project has been sensitive to river discharge, while the response following the downstream reclamation has been predominantly a tidal response. In both cases, there was a discernible influence in the central segment of the South Branch, where shoal movement, collapse and regeneration have been very dynamic. Consequently, the influence of these interventions has extended downstream and upstream by approximately 20 km and 30 km, respectively.

Discharge records from Datong station show that river floods have occurred at various intervals throughout the study period. This remains the case for post-completion of the Three Gorges Dam, although the

magnitude of the peak is now controlled. Particularly large storm events were recorded in 1954, 1968/69, 1973, 1977, 1983, 1995/96 and 1998/99 (Luan et al., 2016). Hence five events fall within the first interval (1958–1987), two are in the central interval and two are in the last interval (1997–2007). The events that occurred in 1983, 1995, 1996, 1998 and 1999 were more extreme. These events are all capable of moving substantial volumes of sediment and would have contributed to the observed changes. However, assuming that large floods perturb the system away from the ‘most probable state’, the timing of events is inconsistent with the observed changes in state, even allowing for some lag in the response. Furthermore, a clear negative perturbation (less efficient) is evident in the first and last intervals (Fig. 7d). The response in the first interval is clearly sensitive to river flow conditions, whereas the response in the last interval is not. If floods were the cause, the observed response should be the same in both intervals. Therefore, it is inferred that river and tide impacts are superimposed with reclamations on the South Branch evolution.

Moreover, the narrowing of the channels around Xuliujing restricts the river discharge at the upstream end of the South Branch. Such a restriction of the channel is likely to have enhanced the role of high flows in the downstream reach. The observed collapse and reformation of the Baimaoshan shoal indicate a response 20 km downstream from Xuliujing, and the system moves away from the ‘most probable state’. Furthermore, the modeled river flood and spate conditions disturbed the system away from equilibrium by 3–6% in 1958, while this value was reduced to 2–4% in 2007 for the same flow conditions. This is most likely a consequence of the constraints on the upstream section imposed by the reclamation around Xuliujing, which fixed the banks and caused subtidal channel deepening.

Similarly, the progressive enlargement of Changxing Island and construction of the Qingcaosha Reservoir (at the lower end) after 1997 led to the mouth becoming narrower and deeper. As a result, the balance between the river and tides has also been changed by reducing the amount of tidal energy entering the estuary. With a reduction in tidal flow relative to river flow, the location of the river-tidal transition is estimated to have gradually moved downstream from approximately 45 km from the mouth in 1958 to 30 km in 2007, suggesting that the location of tidal flow reversals and turbidity maxima may have also moved downstream (Li et al., 2012; Gong et al., 2012). These estimates are slightly downstream of the crossover reported by Yang et al. (2017) but well within the ‘mixed energy’ zone that was defined in their study (see Fig. 7 of Yang et al., 2017).

4.3. Contributions from river floods and reclamations

Attributing the cause of morphological change is not straightforward but is inferred from the changes in state, which are suggested by the results. The percent difference in energy flux along the chainage from the defined most probable state locally quantifies the equilibrium state of the South Branch (Fig. 6). Moreover, integrating the percent differences over the entire South Branch reveals the similarity in the system behavior between global entropy production (Fig. 7d) and energy dissipation (Fig. 7c) changes over time. These results provide a basis for inferring the probable causes of the observed changes.

The entropy argument in Fig. 7d suggests that prior to the occurrence of large-scale human activities in 1958, typical flood (35,000 m³/s) and spate (60,000 m³/s) conditions had moved the system away from equilibrium by 3–6% compared with no runoff and dry season conditions, while the effect of human interventions had further moved the system away from equilibrium by 1.5–2% between 1958 and 1987, when large scale Xuliujing reclamations occurred, and by approximately 1% between 1997 and 2007, when the Qingcaosha Reservoir was constructed. During the intervention period (1987–1997), the natural forcing was able to restore some of the lost efficiency by 2–3.5%. Therefore, it can be concluded that river flood and spate conditions disturbed the system away from equilibrium by 3–6% in

1958, while this value was reduced to 2–4% in 2007 after a series of reclamation projects stabilized the node and deepened the subtidal zone. Taken together, it can be concluded that human activities in the South Branch disturbed the system away from equilibrium by 2.5–3% in total, although they also helped reduce the river flood disturbance by 1–2%. Moreover, the proportion analysis also indicates the contribution of nonequilibrium for each component, i.e., under typical wet conditions (35,000 m³/s), river floods contributed 55% of the system disturbance, and the Xuliujing reclamation and Qingcaosha Reservoir contributed 28% and 17%, respectively. However, when the river discharge increased to 60,000 m³/s, the disturbance caused by river flooding increased significantly to 70%, while the proportion from the Xuliujing reclamation and Qingcaosha Reservoir decreased to only 20% and 10%, respectively.

4.4. South Branch stability

From the above information, we surmise that the inner reach was close to equilibrium in the early 1960s, while the middle and outer reaches were relatively inefficient at that time because of excessive sediment (possibly caused by the large flood in 1954, as discussed by Wang et al., 2013); the channels were undersized with a network of shoals and channels. Thereafter, large-scale reclamation projects paced the South Branch in a period of continuous change, which can be summarized in three stages.

Stage 1: The effect of the reclamation works around Xuliujing, combined with a number of river floods, narrowed and deepened the channels, restored the Baimaoshan shoal and exported a substantial amount of sediment. This large perturbation resulted in the inner reach moving away from equilibrium and the downstream segments adjusting to be more energy efficient. Hence, there was a well-defined post-reclamation adjustment downstream. The fact that the system was more inefficient under high flow conditions after the reclamation activities suggests that it was the high flow conditions that provided the energy for the system to adjust and recoup some of the lost efficiency. **Stage 2:** Between 1987 and 1997, the system recovered, infilling Segment 1 and enlarging Segments 2 and 3 with well-defined shoal-channel development. Thus, by 1997, the system was moving closer to a more efficient and more probable state. **Stage 3:** Construction of the Qingcaosha Reservoir further reduced tidal energy propagation by constraining the mouth and disturbing the estuary stability over the upstream reach (15–55 km from the mouth). This is suggested to be tidally driven because the system exhibits a move away from the most probable state, regardless of the flow conditions (Fig. 7d). Further investigation is needed to establish whether this perturbation will be restored to a more efficient state after 2007.

Overall, there has been a move away from the theoretical optimum at both ends of the South Branch, which we assert is primarily in response to human interventions, with a move back toward the optimum under the prevailing natural conditions (river and tide). If this concept is correct, it confirms that the estuary stability is conditioned by the constraints on the system and that human interventions are now of a sufficiently large scale to be significant at the system scale (Zhou et al., 2017). Such constraints inevitably mean that not all states are accessible, and in turn, this limits the ability for entropy production to be minimized. However, the different responses and coadjustment of the three segments highlight the ability of the system to make use of its many degrees of freedom to adjust and thus restore the overall efficiency of the system.

4.5. Uncertainty analysis

Historical bathymetry reconstruction combined with a reconstruction of river-tide hydraulics has been used to examine hypsometric and tidal volume changes as well as energy fluxes in the South Branch of the Yangtze estuary. In turn, the latter has been used as a diagnostic tool to

examine the energy dissipation and variance from a theoretically most probable state. In isolation, each method provides useful information. However, in combination, they provide much greater insights into the system dynamics and response to changes. In this study, the distinct characteristics of two large-scale human interventions have allowed for a tentative attribution to be made. These findings are consistent with those of previous research, which highlighted the importance of geological constraints (Townend and Dun, 2000) and entropy-based prediction of morphological change (Nield et al., 2005).

However, the application of this research is limited by the time frequency of available data and the extent of the study area. Projects in the seaward, up-river and North Branch areas may have some influences, although this should be secondary relative to the changes directly imposed on the South Branch. The timing of the inferred response is broad because only four surveys are available. In addition, other processes, such as wind-waves (Zhang et al., 2018a,b), density currents (Yang et al., 2017) and Coriolis force (Li et al., 2011), may also have influences, but as already discussed, these influences are expected to be localized (e.g., near the mouth) or secondary. A future investigation of the response post-2007 would be valuable but will require annual bathymetric measurements, rather than a composite of several years, and this data is difficult to acquire.

5. Conclusions

Currently, a detailed exploration of estuary stability based on energy has only been presented for a limited number of estuary types and none of the size and dynamic variability of the Yangtze estuary. The results presented here provide a more complete insight into the system dynamics over short-term (seasonal) and medium-term (decadal) time scales in response to environmental (natural and man-made) perturbations. In summary:

- 1) The morphological evolution of South Branch during the examined period (1958–2007) shows substantial changes under massive human reclamations whereby the surface area has decreased by 22%, while the total volume has reduced by 11%. In total, area and volume by reclamations are slightly greater than the changes in estuary size, suggesting that the losses have been offset by a small amount of widening and deepening. The effect of SLR on the water volume is negligible in comparison to the total morphological change.
- 2) Two massive reclamation projects have occurred within the South Branch, which were clearly separated in space and time, i.e., the Xuliujing reclamations in the upstream end and at the beginning of the study period (before the 1980s) and the Qingcaosha Reservoir construction toward the mouth at the end of the study period (2007). Collectively, these activities contributed 28% and 17% of the system nonequilibrium under typical wet season conditions, with river flooding contributing 55%; the contributions decreased to only 20% and 10% of the system nonequilibrium when river flooding increases to spate conditions, with the latter accounts for 70%.
- 3) The energy input from the ocean has reduced over the last 50 years, albeit with a small increase in 2007. Coupled with the morphological changes (including the imposed changes due to the reclamation), the model results suggest that there has been a shift in the river-tide transition to more seaward direction.
- 4) As each end of South Branch was restricted by reclamations, the morphology, hydrology and energy exhibited a consistent and progressive response between segments. The mechanism of change in response to the two interventions was distinct. The changes resulting from the Xuliujing reclamations were largely dominated by changes in the response to varying river flows, and the morphological adjustments propagated downstream by approximately 20 km to around Baibaosha. In contrast, the response to the Changjiang

Island expansion and construction of the Qingcaosha Reservoir was largely driven by tidal actions, and the adjustments propagated upstream by approximately 30 km to around Biandansha in the middle reach.

Our analysis of energy dissipation and the most probable state suggests clear perturbation and subsequent restoration toward new most probable states. The Xuliujing reclamation project and Qingcaosha Reservoir disturbed the system away from equilibrium with increased entropy. However, the energy dissipation and entropy measures both indicated that the South Branch as a whole was starting to re-establish a more efficient system under actions of prevailing natural forces from 1987 to 1997. Therefore, further adjustment after 2007 within the South Branch is expected and it will be interesting to see if the system can once again adjust to restore the lost efficiency.

Acknowledgments

This research is supported by the National Natural Science Foundation of China (41701001), Key projects of intergovernmental science and technology innovation cooperation of the Ministry of Science and Technology in China (2018YFE0109900), China Postdoctoral Science Foundation (2018M630414), NSFC-NOW-EPSRC Joint Research Projects (51761135024) and Shanghai International Cooperation Project (19230712400). The authors would like to express their appreciation to editor and two anonymous reviewers, who provided helpful comments to improve the manuscript. The marine bathymetry data of this study is available from the Shanghai Institute of Geological Survey (<http://www.silrs.com>, accessed on 11th August, 2019). The hydrological data of this study is available from the National Climatic Centre of the Chinese Meteorological Administration (<http://cdc.cma.gov.cn>, accessed on 11th August, 2019).

Appendix A. Supplementary data

Supplementary data to this article can be found online at <https://doi.org/10.1016/j.ecss.2019.106383>.

References

- Bodge, K.R., 1992. Representing equilibrium beach profiles with an exponential expression. *J. Coast. Res.* 8 (1), 47–55.
- Cooper, J.A.G., 2002. The role of extreme floods in estuary-coastal behaviour: contrasts between river- and tide-dominated microtidal estuaries. *Sediment. Geol.* 150 (1–2), 123–137.
- Dai, Z., Liu, J.T., Fu, G., Xie, H., 2013. A thirteen-year record of bathymetric changes in the North Passage, Changjiang (Yangtze) estuary. *Geomorphology* 187, 101–107.
- Dai, Z., Fagherazzi, S., Mei, X., Chen, J., Meng, Y., 2016. Linking the infilling of the north Branch in the Changjiang (Yangtze) estuary to anthropogenic activities from 1958 to 2013. *Mar. Geol.* 379, 1–12.
- Dalrymple, R.W., Choi, K., 2007. Morphologic and facies trends through the fluvial-marine transition in tide-dominated depositional systems: a schematic framework for environmental and sequence-stratigraphic interpretation. *Earth Sci. Rev.* 81 (3–4), 135–174.
- Dronkers, J., 1986. Tidal asymmetry and estuarine morphology. *Neth. J. Sea Res.* 20 (2–3), 117–131.
- Gao, S., 2013. Holocene shelf-coastal sedimentary systems associated with the Changjiang River: an overview. *Acta Oceanol. Sin.* 32 (12), 4–12.
- Ge, J., Ding, P., Chen, C., Hu, S., Fu, G., Wu, L., 2013. An integrated East China Sea-Changjiang Estuary model system with aim at resolving multi-scale regional-shelf-estuarine dynamics. *Ocean Dyn.* 63 (8), 881–900.
- Gong, Z., Zhang, C.K., Wan, L.M., Zuo, J.C., 2012. Tidal level response to sea-level rise in the Yangtze estuary. *China Ocean Eng.* 26 (1), 109–122.
- Guo, C., Zhu, J., 2015. Impact of Qingcaosha Reservoir project on the bed erosion and deposition nearby the water area (in Chinese). *J. Mar. Sci.* 33 (3), 34–41.
- Guo, L., van der Wegen, M., Roelvink, J.A., He, Q., 2014. The role of river flow and tidal asymmetry on 1-D estuarine morphodynamics. *J. Geophys. Res.: Earth Surf.* 119 (11) 2014JF003110.
- Haigh, I.D., Eliot, M., Pattiaratchi, C., 2011. Global influences of the 18.61 year nodal cycle and 8.85 year cycle of lunar perigee on high tidal levels. *J. Geophys. Res.: Oceans* 116 (C6), C06025.
- Huang, H.Q., Deng, C., Nanson, G.C., Fan, B., Liu, X., Liu, T., Ma, Y., 2014. A test of equilibrium theory and a demonstration of its practical application for predicting the

- morphodynamics of the Yangtze river. *Earth Surf. Process. Landforms* 39 (5), 669–675.
- Langbein, W.B., 1963. The hydraulic geometry of a shallow estuary. *Bull. Int. Assoc. Sci. Hydrol.* (8), 84–94.
- Latteux, B., 1995. Techniques for long-term morphological simulation under tidal action. *Mar. Geol.* 126 (1–4), 129–141.
- Leopold, L.B., Langbein, W.B., 1962. The Concept of Entropy in Landscape Evolution. *Theoretical Papers in the Hydrologic and Geomorphic Sciences*, Geological Survey Professional Paper 500-A. pp. 1–18.
- Li, M., Chen, Z., Yin, D., Chen, J., Wang, Z., Sun, Q., 2011. Morphodynamic characteristics of the dextral diversion of the Yangtze River mouth, China: tidal and the Coriolis Force controls. *Earth Surf. Process. Landforms* 36 (5), 641–650.
- Li, P., Yang, S.L., Milliman, J.D., Xu, K.H., Qin, W.H., Wu, C.S., Chen, Y.P., Shi, B.W., 2012. Spatial, temporal, and human-induced variations in suspended sediment concentration in the surface waters of the Yangtze Estuary and adjacent coastal areas. *Estuar. Coasts* 35 (5), 1316–1327.
- Luan, H.L., Ding, P.X., Wang, Z.B., Ge, J.Z., Yang, S.L., 2016. Decadal morphological evolution of the Yangtze Estuary in response to river input changes and estuarine engineering projects. *Geomorphology* 265, 12–23.
- Liu, Z., 1992. Modern sea level changes of the eastern china seas and their influences on coastal areas. *J. Environ. Sci.* 4 (1), 52–59.
- Luan, H.L., Ding, P.X., Wang, Z.B., Ge, J.Z., 2017. Process-based morphodynamic modeling of the Yangtze Estuary at a decadal timescale: controls on estuarine evolution and future trends. *Geomorphology* 290, 347–364.
- McLaren, P., 2013. Sediment trend analysis (STA[®]): kinematic vs. Dynamic modeling. *J. Coast. Res.* 30 (3), 429–437.
- McLaren, P., 2016. The environmental implications of sediment transport in the waters of Prince Rupert, British Columbia, Canada: a comparison between kinematic and dynamic approaches. *J. Coast. Res.* 32 (3), 465–482.
- Nicholls, R.J., French, J.R., van Maanen, B., 2016. Simulating decadal coastal morphodynamics. *Geomorphology* 256, 1–2.
- Nield, J.M., Walker, D.J., Lambert, M.F., 2005. Two-dimensional equilibrium morphological modelling of a tidal inlet: an entropy based approach. *Ocean Dyn.* 55 (5–6), 549–558.
- Nordhaus, I., Roelke, D.L., Vaquer-Sunyer, R., Winter, C., 2018. Coastal systems in transition: from a 'natural' to an 'anthropogenically-modified' state. *Estuar. Coast Shelf Sci.* 211, 1–5.
- Rodríguez-Iturbe, I., Rinaldo, A., 1997. *Fractal River Basins: Chance and Self-Organisation*. Cambridge University Press, Cambridge, pp. 1–67.
- Shi, Y., Zhu, J., Xie, Z., Ji, Z., Jiang, Z., Yang, G., 2000. Prediction and prevention of the impacts of sea level rise on the Yangtze River Delta and its adjacent areas. *Sci. China Ser. D Earth Sci.* 43 (4), 412–422.
- Syvitski, J.P.M., Kettner, A.J., Overeem, I., Hutton, E.W.H., Hannon, M.T., Brakenridge, G.R., Day, J., Vörösmarty, C., Saito, Y., Giosan, L., Nicholls, R.J., 2009. Sinking deltas due to human activities. *Nat. Geosci.* 2, 681–686.
- Tejedor, A., Longjas, A., Edmonds, D.A., Zaliapin, I., Georgiou, T.T., Rinaldo, A., Foufoula-Georgiou, E., 2017. Entropy and optimality in river deltas. *Proc. Natl. Acad. Sci. U. S. A.* 114 (44), 11651–11656.
- Townend, I., Dun, R., 2000. A diagnostic tool to study long-term changes in estuary morphology. *Geol. Soc. Lond. Special Publications* 2000.
- Townend, I.H., Wang, Z.B., Rees, J.G., 2007. Millennial to annual volume changes in the humber estuary. *Proc. Math. Phys. Eng. Sci.* 463 (2079), 837–854.
- van der Wegen, M., Wang, Z.B., Savenije, H.H.G., Roelvink, J.A., 2008. Long-term morphodynamic evolution and energy dissipation in a coastal plain, tidal embayment. *J. Geophys. Res.: Earth Surf.* 113 (F3), F03001.
- van der Wegen, M., Roelvink, J.A., 2008. Long-term morphodynamic evolution of a tidal embayment using a two-dimensional, process-based model. *J. Geophys. Res.: Oceans* 113 (C3), 0148–0227.
- Wang, Y., Dong, P., Oguchi, T., Chen, S., Shen, H., 2013. Long-term (1842–2006) morphological change and equilibrium state of the Changjiang (Yangtze) Estuary, China. *Cont. Shelf Res.* 56, 71–81.
- Wang, Y., Ridd, P.V., Wu, H., Wu, J., Shen, H., 2008. Long-term morphodynamic evolution and the equilibrium mechanism of a flood channel in the Yangtze Estuary (China). *Geomorphology* 99 (1–4), 130–138.
- Wang, Z.B., Townend, I.H., 2012. Influence of the nodal tide on the morphological response of estuaries. *Marine Geol.* 291–294, 73–82.
- Wu, H.L., Shen, H.T., Wu, J.X., 2002. Relationships among depth datum levels in the Yangtze Estuary (in Chinese). *Ocean Eng.* 20 (1), 69–74.
- Xu, K., Milliman, J.D., 2009. Seasonal variations of sediment discharge from the Yangtze River before and after impoundment of the three Gorges dam. *Geomorphology* 104 (3–4), 276–283.
- Yang, C.T., 1971. Potential energy and stream morphology. *Water Resour. Res.* 7 (2), 311–322.
- Yang, H.F., Yang, S.L., Xu, K.H., 2017. River-sea transitions of sediment dynamics: a case study of the tide-impacted Yangtze River estuary. *Estuar. Coast Shelf Sci.* 196, 207–216.
- Yang, S.L., Zhang, J., Xu, X.J., 2007. Influence of the Three Gorges Dam on downstream delivery of sediment and its environmental implications, Yangtze river. *Geophys. Res. Lett.* 34 (10), F02003F5.
- Zhang, M., Townend, I., Zhou, Y., Cai, H., 2016a. Seasonal variation of river and tide energy in the Yangtze estuary, China. *Earth Surf. Process. Landforms* 41 (1), 98–116.
- Zhang, M., Townend, I.H., Cai, H., Zhou, Y., 2016b. Seasonal variation of tidal prism and energy in the Changjiang River estuary: a numerical study. *Chin. J. Oceanol. Limnol.* (01), 219–230.
- Zhang, M., Townend, I., Cai, H., He, J., Mei, X., 2018a. The influence of seasonal climate on the morphology of the mouth-bar in the Yangtze Estuary, China. *Cont. Shelf Res.* 153 (Suppl. C), 30–49.
- Zhang, X., Fagherazzi, S., Leonardi, N., Li, J., 2018b. A positive feedback between sediment deposition and tidal prism may affect the morphodynamic evolution of tidal deltas. *J. Geophys. Res.: Earth Surf.* 123 (11), 2767–2783.
- Zhao, J., Guo, L., He, Q., Wang, Z.B., van Maren, D.S., Wang, X., 2018. An analysis on half century morphological changes in the Changjiang Estuary: spatial variability under natural processes and human intervention. *J. Mar. Syst.* 181, 25–36.
- Zhou, Z., Coco, G., Jiménez, M., Olabarrieta, M., van der Wegen, M., Townend, I., 2014. Morphodynamics of river-influenced back-barrier tidal basins: the role of landscape and hydrodynamic settings. *Water Resour. Res.* 50 (12), 9514–9535.
- Zhou, Z., Coco, G., Townend, I., Olabarrieta, M., van der Wegen, M., Gong, Z., D Alpaos, A., Gao, S., Jaffe, B.E., Gelfenbaum, G., He, Q., Wang, Y., Lanzoni, S., Wang, Z., Winterwerp, H., Zhang, C., 2017. Is "morphodynamic equilibrium" an oxymoron? *Earth Sci. Rev.* 165, 257–267.
- Zhu, J., Gu, Y., Wu, H., 2013. Determination of the period not suitable for taking domestic water supply to the Qincaosha Reservoir near Changjiang River estuary (in Chinese). *Oceanol. Limnol. Sinica* 05, 1138–1145.
- Zhu, L., He, Q., Shen, J., Wang, Y., 2016. The influence of human activities on morphodynamics and alteration of sediment source and sink in the Changjiang estuary. *Geomorphology* 273, 52–62.